Available online at www.sciencedirect.com
ScienceDirect
Trans. Nonferrous Met. Soc. China 21(2011) 1052−1060
Transactions of Nonferrous Metals Society of China
www.tnmsc.cn

Oxidation behaviors of electrodeposited nickel-cobalt coatings in air at 960 °C

ZHOU Ke-chao, MA Li, LI Zhi-you

State Key Laboratory of Powder Metallurgy, Central South University, Changsha 410083, China

Received 18 June 2010; accepted 21 October 2010

Abstract: Ni coating and Ni-Co alloy coatings were produced by adjusting the composition of the plating solution using a direct current electrodepositing process. The oxidation behaviors of nickel and nickel-cobalt alloys in air at 960 °C were studied by thermogravimetric (TG) analyzer and then the formed oxide scales were examined by scanning electron microscopy/energy dispersive spectroscopy (SEM/EDS), X-ray diffractometry (XRD), and Raman spectroscopy. The scale morphologies, composition, grain size and mechanism of oxidation were discussed in detail. The results show that oxidation rates of Ni, Ni-7%Co (mass fraction) and Ni-15%Co generally follow parabolic relationship, whereas that of Ni-30% Co alloy follows cubic relationship. The higher the Co content of the alloys is, the faster the oxidation rate is. Metal concentration profiles reveal cobalt depletion in the alloy surface beneath oxide scales, and a progressive enrichment in cobalt towards the outer surface of the scale.
Key words: nickel-cobalt alloys; electrodeposition; high temperature oxidation

1 Introduction

Nickel-based alloys are used widely in aerospace, energy generation and corrosion protection, especially in corrosive environments at high temperatures[1−2]. Among these materials, Ni-Co alloys have gained popularity because they exhibit functional properties other than corrosion resistance, such as magnetic materials[3] and electro catalysis in hydrometallurgy[4]. It was found that the mixed cobalt-nickel oxides, which were fabricated by spin casting from solution precursors, have higher conductivities of five orders of magnitudes more than either of the two end members, containing Co and Ni in a spinel crystal structure[5]. Due to their extraordinary hardness, good conductivities of their oxides, combined with a high corrosion resistance, Ni-Co alloys are under consideration as a potential system for hard chromium replacement and high-temperature conductive materials. Therefore, it is very significant to study their high temperature oxidation and corrosion performance. However, great attention was given to the oxidation of pure nickel and pure cobalt. There was surprisingly little study on the behavior of the binary alloys of the two metals. Such single-phase alloys produce a single-phase oxide (Ni, Co)O at 900−1 000 °C, presenting for an almost uniquely simple alloy oxidation situation. But the surface topography and grain size distribution through scales were rarely studied. In addition, the oxidation behavior of Ni-Co coatings was also rarely reported. Ni-Co alloys can be easily produced by electrodeposition from aqueous media in a broad variety of alloy compositions[6]. As a consequence, this investigation on the oxidation behavior of Ni-Co coatings is also significant for the wide application of electrodeposited materials.

In the present work, the oxidation behaviors of electrodeposited nickel-cobalt coatings at 960 °C were studied; the morphology, microstructure, composition and grain size of the formed oxide scales were carefully examined and then regulations of scale growth were discussed.

2 Experimental

Samples with dimensions of 30 mm×30 mm×2 mm were cut from a pure electrolytic nickel plate (≥99.9%), whose compositions are listed in Table 1. Then they were abraded down to 1000 grit SiC paper. Ni and Ni-Co alloy coatings with thickness of 40−50 μm were prepared

Foundation item: Project (2005CB623703) supported by the National Basic Research Program of China; Project (50474051) supported by the National Natural Science Foundation of China; Project (CX2009B032) supported by Innovation Foundation for Postgraduate of Hunan Province, China; Project (ZKJ2008018) supported by the Precious Apparatus Open Share Foundation of Central South University, China; Project (2009ybfz02) supported by the Outstanding Doctoral Dissertation Support Foundation of Central South University, China
Corresponding author: ZHOU Ke-chao; Tel: +86-731-88836264; E-mail: zhoukcz@csu.edu.cn
DOI: 10.1016/S1003-6326(11)60821-2

Table 1 Chemical composition of pure electrolytic nickel plate (mass fraction, %)

Ni	Co	C	Cu	Fe	S
≥99.9	≤0.1	≤0.005	≤0.003	≤0.000 7	≤0.000 5

by direct current electrodeposition. Coatings were deposited from Watt baths (Table 2) at (45±3) °C. pH value of the bath was adjusted to 4.5 using H_2SO_4 or $NH_3{\cdot}H_2O$ solution. Those substrates were ultrasonically cleaned in ethanol, acetone, and distilled water for 10 min, respectively, activated in 10% H_2SO_4 for 30 s, washed in distilled water, and finally, immersed immediately in the plating bath to allow the electrodeposition of the target coatings. During the deposition process, the plating electrolyte was agitated with a magnetron stirrer. The depositing current density was adjusted to 2.5 A/dm^2. All solutions were prepared using distilled water. At least three specimens for each type were deposited under the same conditions. The results presented were representative of those found for all specimens subjected to a given parameter set.

The phase constituent of the deposits was characterized using an X-ray diffractometer (RIGAKU/MAX-3A) with Cu K_α radiation ($\lambda_{Cu\text{-}K\alpha}$=0.154 nm). The scan rate was 8(˚)/min and 2θ ranged from 20° to 90°. The texture coefficient was analyzed using the X-ray diffraction pattern. For the purpose of qualitatively determining the preferential crystalline orientation of the deposits, the texture coefficient ($T_{(hkl)}$) is used, which is defined as[7]

$$T_{(hkl)}=\frac{I_{(hkl)}/I_{0(hkl)}}{\sum_{i=1}^{n} I_{(hkl)}/I_{0(hkl)}}\times 100\% \quad (1)$$

where $I_{(hkl)}$ and $I_{0(hkl)}$ are the diffraction intensities of the (*hkl*) plane measured in the diffractogram for the deposited coating and the standard Ni powder sample, respectively. There are only three basic reflection lines for the Ni to be considered, (111), (200) and (220), since the diffraction lines of (222) and (400) are the second-order diffraction lines of the (111) and (200) planes, respectively. $T_{(hkl)}$ denotes the percentage of the relative intensity of a given orientation (*hkl*) among the 3 crystallographic orientations of each sample, while a preferential orientation of the (*hkl*) plane is indicated by a value of $T_{(hkl)}$>33.3%.

The coated samples were oxidized thermally in a muffle stove in air at 960 °C for 18 h. The mass changes were measured continuously by a TherMax 700 thermogravimetric analyzer (TGA) (Thermo-Cahn, USA) with a sensitivity of 0.3 μg.

After oxidation, the phase constituents, surface and cross-sectional morphologies of the scale were examined with X-ray diffractometer (XRD), scanning electron microscope (SEM), energy dispersive spectroscope (EDS) and Raman spectroscope, at an excitation wavelength of 488 nm (argon ion laser, output power of 100 mW).

3 Results and discussion

3.1 Microstructures of as-deposited Ni and Ni-Co coatings

XRD analysis was utilized to characterize the deposited Ni and Ni-Co coatings with different Co contents (7%−30%). The deposited Co concentration was varied by changing the Co salt composition in the plating bath. Representative XRD patterns are shown in Fig.1. Table 3 shows the characteristic XRD data for the

Table 2 Composition of plating baths

Coating	$c(NiSO_4{\cdot}6H_2O)$/(mol·L^{-1})	$c(CoSO_4{\cdot}7H_2O)$/(mol·L^{-1})	$c(NiCl_2{\cdot}6H_2O)$/(mol·L^{-1})	$c(H_3BO_3)$/(mol·L^{-1})	pH
Ni	0.95	−	0.19	0.40	4.5
Ni-7%Co	0.95	0.01	0.19	0.40	4.5
Ni-15%Co	0.95	0.03	0.19	0.40	4.5
Ni-30%Co	0.95	0.05	0.19	0.40	4.5

Table 3 Position (2θ), full width at half-maximum (FWHM), d(=2sinθ/λ), texture coefficient of (111) plane ($T_{(111)}$) obtained from XRD patterns for different samples

Sample	2θ/(°)			FWHM(111) /Å	d/Å			$T_{(111)}$/%
	(111)	(200)	(220)		(111)	(200)	(220)	
Ni(PDF)	44.48	51.83	76.35		2.0352	1.7625	1.2463	33.3
Ni	44.40	51.74	76.32	0.174	2.0387	1.7653	1.2467	40.7
Ni-7%Co	44.38	51.74	76.26	0.181	2.0395	1.7654	1.2476	45.6
Ni-15%Co	44.34	51.72	76.24	0.212	2.0412	1.7659	1.2478	57.1
Ni-30%Co	44.28	51.70	76.18	0.272	2.0437	1.7667	1.2486	40.6

prepared materials. XRD patterns confirm that the electrodeposited Ni-Co alloy coating is composed of a Ni-Co solid solution (see Fig.1). The texture coefficients of (111) planes are slightly larger than 33.3%, indicating very weak preferential texture existing in these coatings. The texture coefficients of (111) planes do not change obviously in 40%−57% as the Co concentration is increased for the deposited coatings. However, the diffraction peaks of (111), (200) and (220) planes shift to smaller 2θ values and d values of all planes become larger as the deposited Co concentration is increased. Both the results are due to more cobalt atoms incorporating in nickel lattice. In addition, a steady increase in FWHM of the main peak of (111) from 0.174 to 0.272 Å is evident as the Co concentration increases in the alloys from 0 to 30%, indicating that their grain size becomes small[8].

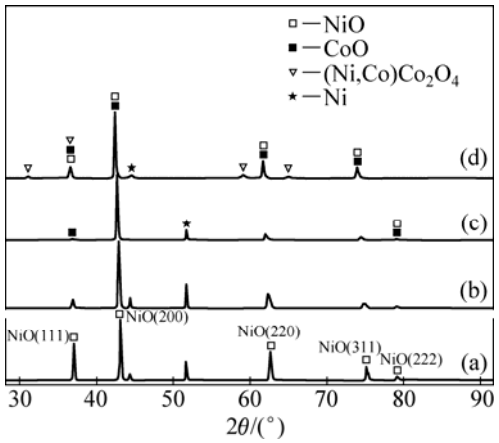

Fig.2 XRD patterns of oxides scales formed on coatings in air at 960 °C for 18 h: (a) Ni; (b) Ni-7%Co; (c) Ni-15%Co; (d) Ni-30%Co

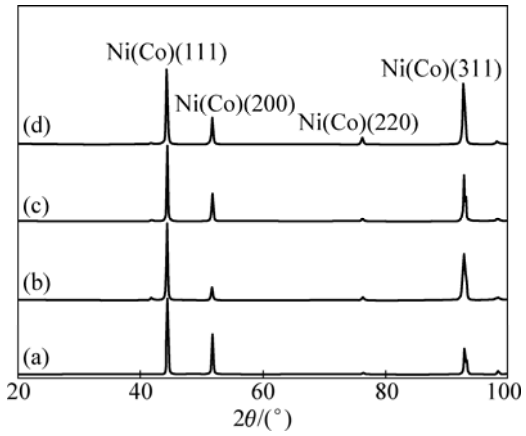

Fig.1 XRD patterns of coatings: (a) Ni; (b) Ni-7%Co; (c) Ni-15%Co; (d) Ni-30%Co

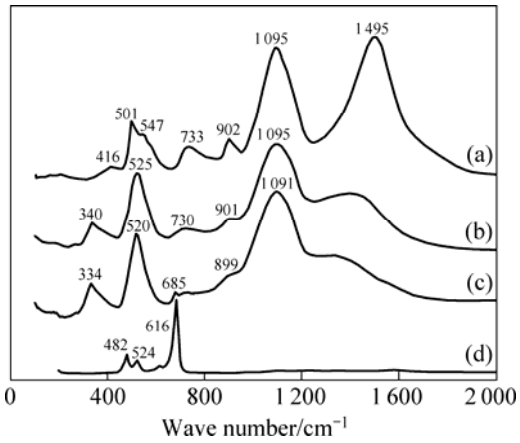

Fig.3 Raman patterns of top oxide layers formed on coatings in air at 960 °C for 18 h: (a) Ni; (b) Ni-7%Co; (c) Ni-15%Co; (d) Ni-30%Co

3.2 Composition and phase constituents of oxide scales

The phase constituents of oxide scales formed on the coating surfaces were also investigated by X-ray diffractometry (XRD). Figure 2 shows XRD patterns of the coatings oxidized in air at 960 °C for about 18 h. At a low concentration of Co (7%−15%), the oxide scales of Ni-Co coatings are composed of only Ni(Co)O solid solution. At a high concentration of Co(30%), the oxide scales for Ni-Co coatings are composed of not only Ni(Co)O solid solution phase, but also $(Ni,Co)Co_2O_4$ spinel phases. In addition, the peak positions of Ni(Co)O in these coatings shift to smaller 2θ values as the deposited Co concentration is increased. This can be due to the increased incorporation of CoO phase in NiO lattice, and the difference of lattice parameters of oxides associated with the composition change in (Ni,Co)O.

Figure 3 shows the Raman spectra obtained from the external parts of the oxide scales formed on Ni and Ni-Co coatings. The spectra were obtained from the surfaces of each sample at five different positions. These spectra do not change significantly from place to place on each sample surface. This seems to indicate a homogeneous composition of the layer in the micron scale. The spectrum features of the oxides formed on Ni-30%Co coatings (Fig.3(d)) are obviously different from those of the other three coatings. The observed prominent Raman peaks correspond to E_g (483 cm^{-1}), F_{2g} (524 and 616 cm^{-1}) and A_{1g} (685 cm^{-1}) modes of the Co_3O_4 crystalline phase and are in agreement with the previous reports[9−10]. Therefore, the main oxide formed on the top-layer of Ni-30%Co could be considered Co_3O_4 phase. In addition, the position and relative intensity of the peaks are both somewhat different for the spectra of Ni, Ni-7%Co and Ni-15%Co (Figs.3(a)−(c)) after oxidation at 960 °C. The spectrum (Fig.3(a)) of pure Ni coating after oxidation at 960 °C shows bands at 416, 501, 547, 733, 902, 1 095, 1 495 cm^{-1}, which can be considered representative of NiO

phase. However, for Ni-7%Co and Ni-15%Co coatings (Fig.3(b)−(c)) after oxidation at 960 °C, peaks at 1 495, 501 and 416 cm^{-1} disappeared and broad bands at 334−340 cm^{-1} appeared, which might be due to the incorporation of cubic CoO in NiO crystal lattice. The positions of the main peaks of Ni-7%Co and Ni-15%Co after oxidation at 960°C are somewhat different, which can be associated with their difference either in chemical composition or some aspect of crystallographic structure. These shifted from the positions of the main peaks of 368−400 cm^{-1} in previous studies of bulk CoO[9−10]. This result also confirms that the crystallographic structures of the series of nickel and cobalt oxides can be identified by Raman spectroscopy.

3.3 Oxidation kinetics at 960 °C

Typical oxidation curves for alloys containing 0−30% Co are illustrated by the parabolic plots in Fig.4. In each case, more than one sample were oxidized to check the reproducibility of the kinetic curves, which was found to be within ±5%. Oxidation of pure nickel was used as the basis of comparison for the kinetics. Parabolic kinetics was observed for pure nickel through the entire oxidation period. In the case of the alloy containing 15% Co, an initial non-parabolic transient period of about 500 min was observed before onset of parabolic kinetics. The Ni-30%Co coating shows two-stage kinetics, and the initial stage extends up to ~500 min (Fig.4). The oxidation rate of the alloys increases by the addition of cobalt and subsequently keeps a nearly constant value. The former result shows that ionic diffusion through (Ni,Co)O occurs at an intermediate rate between Ni^{2+} in NiO and Co^{2+} in CoO. The latter result shows them obedience to a parabolic growth relationship despite the presence of a highly complex concentration gradient through the scale. This interesting result is probably because the oxide compositions at the two interfaces are approximately constant with time which fulfils the major requirement of the Wagner derivation. A further interesting feature is that the growth rate of the oxides on Ni-7%Co coating (Fig.4) is nearly the same as that of NiO scale on the pure Ni coating after oxidation for ~500 min (~22 $min^{1/2}$). This indicates that the structure and defects of the oxide scale formed at the initial stage should still exert an influence on subsequent scale development in view of the growth rate and oxide products.

In order to clarify the thermal oxidation kinetics of the Ni-Co in air at 960 °C, the polynomial fitting curves of Fig.4 are shown in Fig.5. The fitting function analysis data in Fig.5 are listed in Table 4. From Fig.5 and Table 4, it can be seen that for Ni, Ni-7%Co and Ni-15%Co coatings, the oxide scale growth follows parabolic law at initial stages. However, Ni-7%Co and Ni-15%Co coatings obey a cubic law at the final stage: $t=A+B(\Delta m/S)+C\cdot(\Delta m/S)^2+D\cdot(\Delta m/S)^3$, where A, B, C and D are constants; t is the oxidation time; and $\Delta m/S$ is mass gain per unit area. For Ni-30%Co coating, the oxide scale growth follows a cubic law at the early stage and follows another cubic law at the final stage of exposure in air at 960 °C. The oxide scale deviates from the parabolic growth law, and the oxide scale growth rate decreasing gradually with the oxidation time has been used to analyze the cubic theory[11]. A change in slope of an Arrhenius-type plot for Ni-7%Co and Ni-15%Co coatings might be attributed to a change in the magnetic properties of the metal substrate from ferromagnetic to paramagnetic at the Curie temperature influencing the diffusion rate of metal ions through the oxide[12]. The electronic properties of the alloy were supposed to influence the concentration gradient of cation vacancies in the film[12].

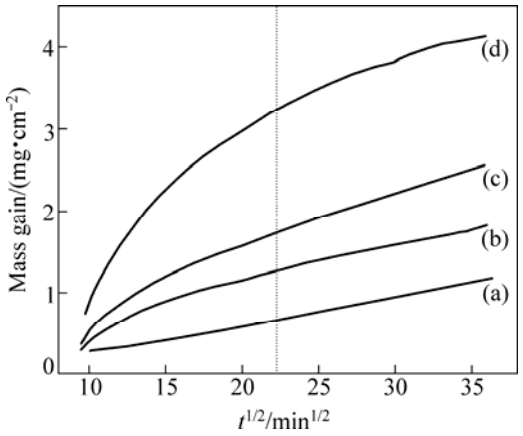

Fig.4 TG curves of coatings in air at 960°C for 18 h: (a) Ni; (b) Ni-7%Co; (c) Ni-15%Co; (d) Ni-30%Co

Table 4 Fitting function analysis of mass gain—time curves for Ni-Co alloys at 960 °C for 18 h

Coating	Time interval/min	A	B	C	D
Ni-7%Co	0−500	−0.32	0.01	-2.24×10^{-5}	1.984×10^{-8}
Ni-15%Co	0−500	−0.47	0.017	-2.99×10^{-5}	2.63×10^{-8}
Ni-30%Co	0−500	−1.04	0.03	-5.81×10^{-5}	4.97×10^{-8}
	500−1 200	1.87	0	-2.15×10^{-6}	4.70×10^{-10}

Fitting curve: $t=A+B(\Delta m/S)+C(\Delta m/S)^2+D(\Delta m/S)^3$.

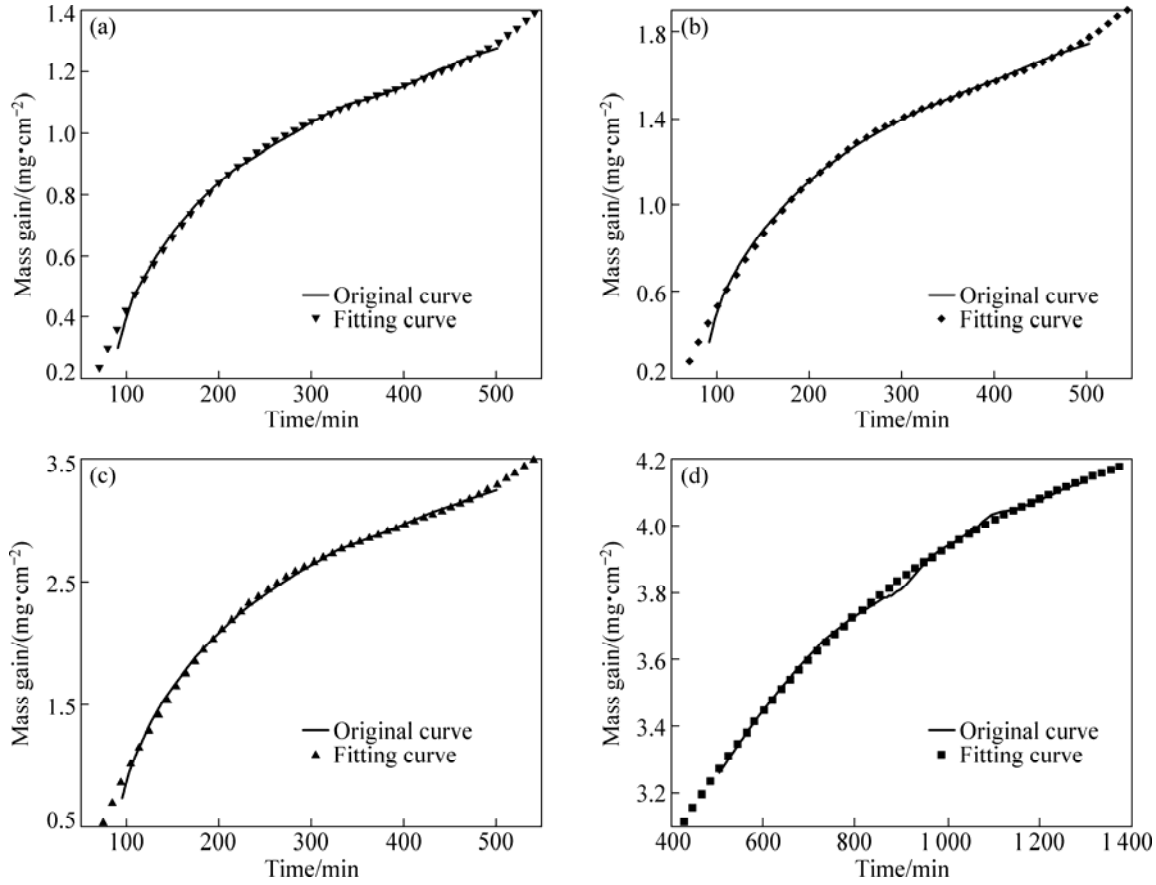

Fig.5 TG curves and their fitting curves of Ni-Co coatings in air at 960 °C: (a) Ni-7%Co; (b) Ni-15%Co; (c), (d) Ni-30%Co

3.4 Oxide scale morphology at 960 °C

Figure 6 shows SEM images of oxide scales after isothermal oxidation of Ni and Ni-Co coatings in air at 960 °C for 18 h. The average grain sizes of all samples are listed in Table 5. Many small pyramid-like oxide grains on the surface are observed in Fig.6. With the increase of Co content, oxide scales with larger grain size are observed, implying the occurrence of an increased lateral growth of the outer layer with the increase of Co content. When the Co mass fraction is up to 30%, lace-like ridges can be observed, which are obviously different from the ridges which were the result of oxide wrinkling induced by release of growth stresses[13] or through microtears in the scale[14]. The formation of lace-like ridges on the oxide scale surface of Ni-30%Co coating suggests a higher diffusivity of elements at the grain boundaries than in grains. EDS elemental mappings for zones *A* and *B* of Fig.6(d) are shown in Fig.7. The EDS analysis also indicates a higher concentration of Co at the grain boundaries. With the help of XRD and Raman analysis, the lace-like ridges can be identified as pure Co_3O_4 phase. The width of lace-like ridges is 250−500 nm (Fig.6(d)). The topography of Ni-30%Co coating after oxidation at 960 °C for 18 h indicates that the grain boundaries and defect sites on the alloy substrate act as preferential growth sites for the external oxide scale (Fig.6(d)). The small crystallites initially formed tend to coalesce and grow, forming bigger grains with a terraced structure (Fig.6(d)). Thus, the oxidation rate at the alloy grain boundaries is different for Ni-Co alloys with different Co contents. This can be due to the difference of elemental diffusivity at the alloy grain boundaries.

Figure 8 presents the corresponding cross-sections of the oxide scales on Ni and Ni-Co coatings. Evidently, thinner oxide scales with thickness of 15−18 μm formed on the Ni, Ni-7%Co and Ni-15%Co coatings; while thicker and porous oxide layer with thickness of about 40 μm grew on Ni-30%Co coating. The whole thicknesses of Ni and Ni-7%Co coatings are nearly the same. This result is consistent with the experimental result in Fig.4. Two distinct layers can be observed in all the oxide scales. The rapid transport of oxygen can be related to the formation of the two-layered oxide scale, composed of equiaxed grains close to the metal/oxide interface, overgrown by columnar grains[15].

It should be noted that the thicknesses of the two layers are also different for all the samples, especially Ni-7%Co and Ni-15%Co coatings. The results are summarized in Table 5. The thickness ratio of the inner

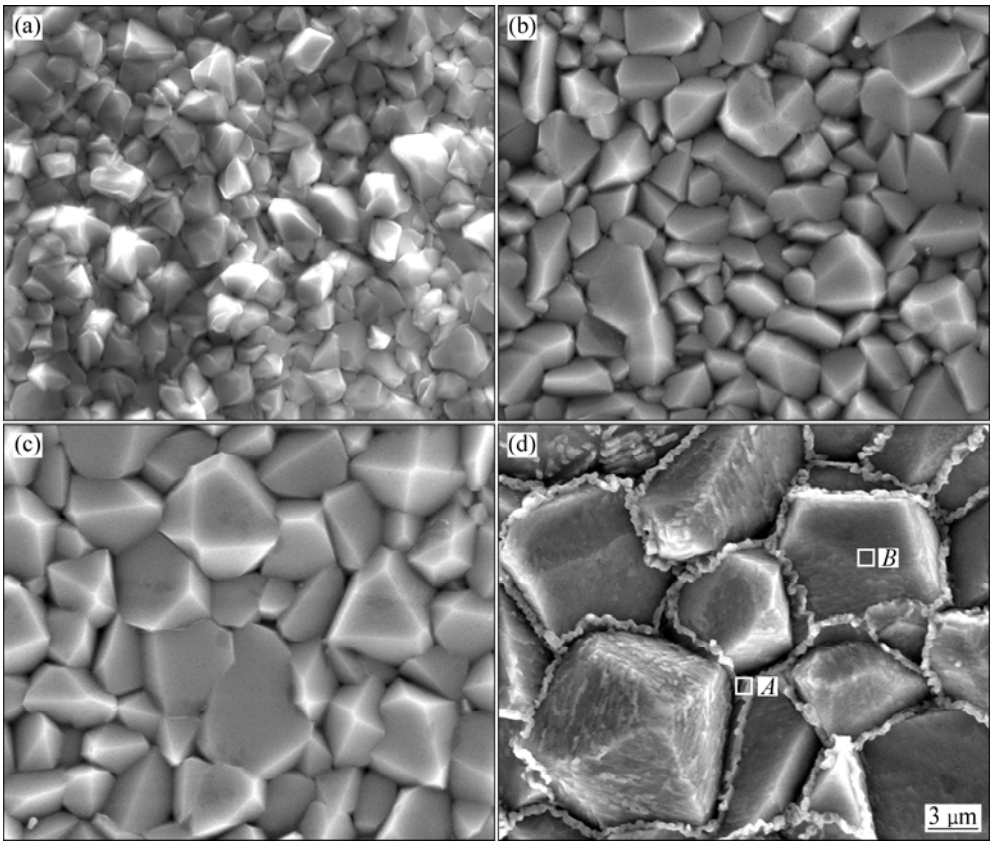

Fig.6 SEM images of oxides formed on surfaces of coatings in air at 960 °C for 18 h: (a) Ni; (b) Ni-7%Co; (c) Ni-15%Co; (d) Ni-30%Co

Table 5 Average oxide grain sizes and thickness ratio of layers in duplex scales

Sample	Average grain size*/μm	Thickness/μm			Thickness ratio of inner to outer layer
		Scale	Inner layer	Outer layer	
Ni	1.5	15	8.2	7.8	10.5:10
Ni-7%Co	2.5	18	8.5	9.5	8.9:10
Ni-15%Co	3.9	17	5.2	11.8	4.4:10
Ni-30%Co	7.8	41	20.2	20.8	9.7:10

* The average grain size in a duplex scale was determined from outer layer.

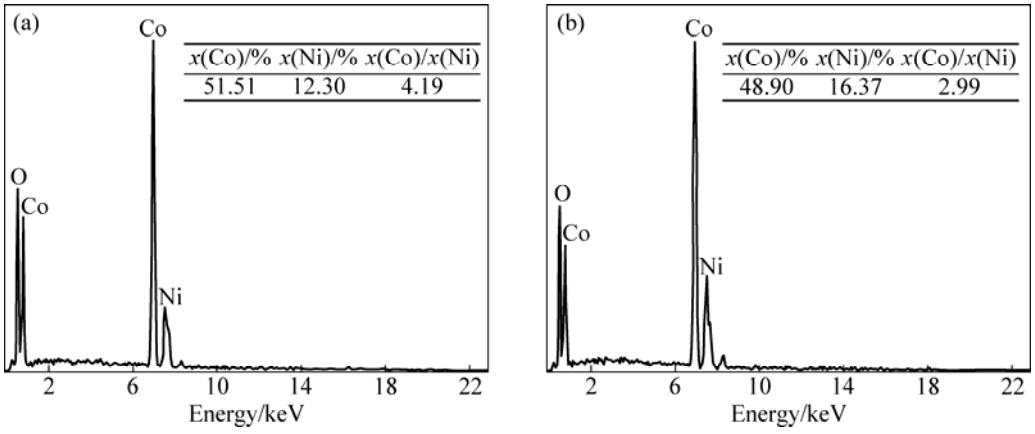

Fig.7 Micro-area elemental analyses in Fig.6(d): (a) Zone *A*; (b) Zone *B*

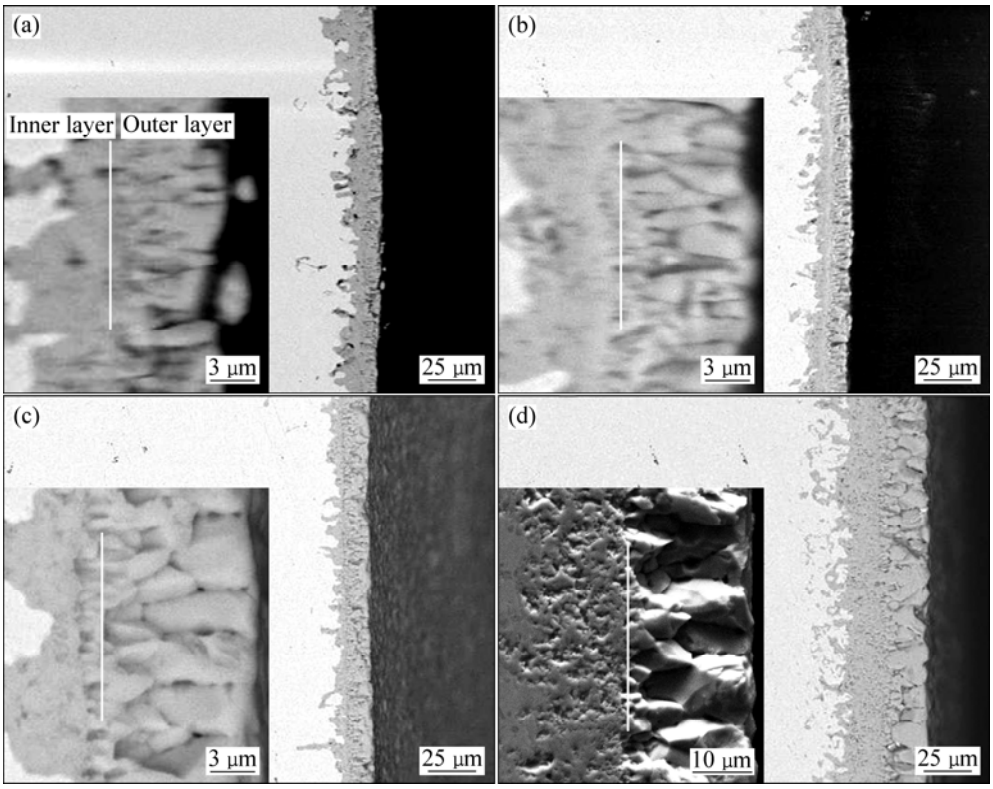

Fig.8 Cross-sectional morphologies of oxide scales formed on coatings in air at 960 °C for 18 h: (a) Ni; (b) Ni-7%Co; (c) Ni-15%Co; (d) Ni-30%Co

to the outer layer is greatly reduced for Ni-15%Co coating, which indicates that the ratio of inward oxygen diffusion to outward cobalt and nickel diffusion is smaller when the cobalt content is up to 15%. The Ni-15%Co coating is slightly thinner than Ni-7%Co coating. However, the mass gain of Ni-15%Co coating is larger than that of Ni-7%Co coating after oxidation in air at 960 °C for 20 h (Fig.4). The outer layers thickness of Ni-15%Co is much thicker than that of Ni-7%Co, whereas the relevant inner layer thickness is thinner than that of Ni-7%Co. These might be due to a higher bulk density for the outer layer, compared with the porous inner layer. More pores are visible in the inner layer of oxide scale of Ni-30%Co coating. Internal oxidation in Ni-30%Co coating is much more pronounced than in the other three coatings (Fig.8(b)). This result might be caused by the following reasons. Firstly, since NiO formed on pure Ni coating through oxidation is a p-type semiconductor of positive ion insufficiency[16], the outward diffusion of positive ions and electrons is preferred during oxidation. As the diffusion of O in NiO is much slower than that of Ni[17], new NiO forms at the NiO/air interface due to Ni ions diffusing through the NiO layer to the NiO/air interface. The activation energy of ion diffusion in the grain boundary is much smaller than that in the lattice[18]. At 400−800 °C, the activation energy of Ni diffusion in the NiO lattice is 254.6 kJ/mol, while the activation energy for the oxidation of Ni is only 159.7 kJ/mol. Compared to the lattice, the grain boundaries can be seen as short-distance ion channels. Thus, nano-grains of Ni-30%Co coating provide important routes for the rapid oxidation at the early stage mainly owing to the increase in grain boundaries. Secondly, since cobalt oxidizes much faster than nickel, and Co^{2+} ions diffuse much faster in CoO than Ni^{2+} ions in NiO, the cobalt-rich scale provides little barrier to oxidation compared with the nickel-rich region appearing in the total film thickness[19]. Furthermore, according to XRD and Raman analyses, Co_3O_4 spinel phase only forms on Ni-30%Co coating after oxidation in air at 960 °C for 18 h. In one interpretation, any increase in oxidation rate from the added cobalt to nickel should be due to Co^{3+} or Co^{4+} ions increasing the number of cation vacancies in NiO. However, since only Co^{2+} ions would exist above 960 °C for Ni-7%Co and Ni-15%Co coatings, no increase in oxidation would be expected in this way. The increase in oxidation rate induced by Co addition was said to be due to greater proportions of CoO in the scale with its accompanying greater growth rate. Electron-probe microanalysis has clearly shown that the oxidation rate is related to diffusion through single or double layer of (Ni,Co)O solid solution with widely varying composition[20]. The formation of many open pores or micro-channels in the oxide scale formed at the initial stage for Ni-30%Co coating will lead to the fast penetration of oxygen

through the oxide layer in subsequent scale development.

Oxide scales formed on Ni-Co alloy at 960 °C are particularly amenable to study by EDS because nickel and cobalt are readily measured, the scales are thick and there is remarkable similarity from place to place over a specimen surface. Typical scales on Ni-30%Co coating were examined in the present case, and shown by BSE images and EDS point scans in several places that the concentration profiles from outer surface to alloy were the same everywhere in a typical region. The EDS results (Fig.9(b)) show that cobalt is intensively depleted at the outer layer/inner layer interface. This depletion resulted from a slight preferential oxidation of cobalt.

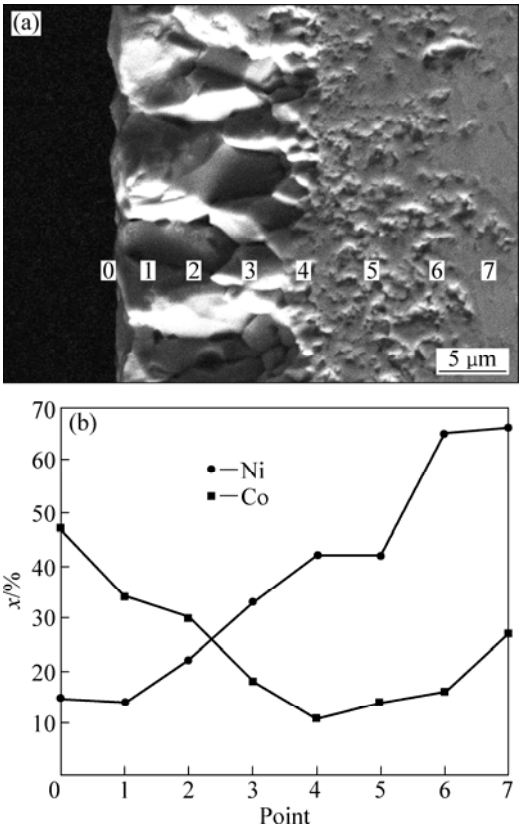

Fig.9 Cross-sectional BSE image (a) of Ni-30%Co coating after being oxidized in air at 960 °C for 18 h and corresponding EDS concentration profile (b)

4 Conclusions

1) Addition of 7% Co to Ni coating has little effect on the oxidation rate, but 30%Co gives a pronounced effect on Ni coating.

2) A parabolic relationship with initial deviations is observed for the oxidation of pure Ni and Ni-7%Co and Ni-15%Co coatings in air at 960 °C.

3) The formed oxide scales consist of two layers, namely, solid solutions of NiO and CoO, but there are some lace-like Co_3O_4 in the Ni-30%Co coating.

References

[1] PENNISI F J, GUPTA D K. Improved plasma-sprayed Ni-Co-Cr-Al-Y and Co-Cr-Al-Y coatings for aircraft gas turbine applications [J]. Thin Solid Films, 1981, 84: 49−58.

[2] UL-HAMID A, MOHAMMED A I, AL-JAROUDI S S, TAWANCY H M, ABBAS N M. Evolution of oxide scale on a Ni-Mo-Cr alloy at 900 °C [J]. Mater Charact, 2007, 58: 13−23.

[3] FENINECH N E, HAMZAOUI R, ELKEDIM O. Structure and magnetic properties of nanocrystalline Co-Ni and Co-Fe mechanically alloyed [J]. Mater Lett, 2003, 57: 4165−4169.

[4] LUPI C, PILONE D. Electrodeposition of nickel-cobalt alloys: The effect of process parameters on energy consumption [J]. Minerals Engineering, 2001, 14: 1403−1410.

[5] WINDISCH C F Jr, FERRIS K F, EXARHOS G J. Synthesis and characterization of transparent conducting oxide cobalt-nickel spinel films [J]. J Vac Sci Technol A, 2001, 19: 1647−1651.

[6] GUO Yue-ping, LI Jian-gong, SUN Xiao-jun. Microstructure and soft magnetic properties of electrodeposited Ni-Co-W alloys [J]. Rare Metal Materials and Engineering, 2009, 38(7): 1292−1295. (in Chinese)

[7] CHEN L, WANG L, ZENG Z, XU T. Influence of pulse frequency on the microstructure and wear resistance of electrodeposited Ni-Al_2O_3 composite coatings [J]. Surf Coat Technol, 2006, 201: 599−605.

[8] KULKARNI A K, SCHULZ K H, LIM T S, KHAN M. Dependence of the sheet resistance of indium-tin-oxide thin films on grain size and grain orientation determined from X-ray diffraction techniques [J]. Thin Solid Films, 1999, 345: 273−277.

[9] TANG C W, WANG C B, CHIEN S H. Characterization of cobalt oxides studied by FT-IR, Raman, TPR and TG-MS [J]. Thermochimica Acta, 2008, 473: 68−72.

[10] WANG C B, LEE C C, BI J L, SIANG J Y, LIU J Y, YEH C T. Study on the steam reforming of ethanol over cobalt oxides [J]. Catalysis Today, 2009, 146: 76−81.

[11] PERALDI R, MONCEAU D, PIERAGGI B. Correlations between growth kinetics and microstructure for scales formed by high-temperature oxidation of pure nickel II. Growth kinetics [J]. Oxid Met, 2002, 58: 275−295.

[12] SMELTZER W W. Oxidation of nickel-cobalt alloys in the range of Curie temperatures [J]. Acta Metallurgica, 1959, 7: 191−198.

[13] TOLPYGO V K, WIEFHAUS H. Segregation at the Al_2O_3-FeCrAl interface during high-temperature oxidation [J]. Oxid Met, 1999, 52: 1−29.

[14] BRUMM M W, GRABKE H J. The oxidation behaviour of NiAl−I. Phase transformations in the alumina scale during oxidation of NiAl and NiAl-Cr alloys [J]. Corrosion Sci, 1992, 33: 1677−1690.

[15] CHEVALIER S, DESSEREY F, LARPIN J P. Oxygen transport during the high temperature oxidation of pure nickel [J]. Oxid Met, 2005, 64: 219−234.

[16] SATO H, MINAMI T, TAKATA S, YAMADA T. Transparent conducting p-type NiO thin films prepared by magnetron sputtering [J]. Thin Solid Films, 1993, 236: 27−31.

[17] DUBOIS C, MONTY C, PHILIBERT J. Oxygen self-diffusion in NiO single crystals [J]. Philosophical Magazine A, 1982, 46: 419−433.

[18] ATKINSON A, TAYLOR R I. The diffusion of 63Ni along grain boundaries in nickel oxide [J]. Philosophical Magazine A, 1981, 43:

979−998.

[19] MOORE W J, LEE J K. Oxidation kinetics of nickel and cobalt [J]. J Chem Phys, 1951, 19: 255.

[20] SHIM M T, MOORE W J. Diffusion of nickel in nickel oxide [J]. J Chem Phys, 1957, 26: 802−804.

电沉积 Ni-Co 涂层在 960 °C 空气中的氧化行为

周科朝，马 莉，李志友

中南大学 粉末冶金国家重点实验室，长沙 410083

摘 要：采用直流电沉积工艺，通过调节电镀液的组成制备 Ni 涂层和 Ni-Co 合金涂层。采用热重(TG)分析金属 Ni 与 Ni-Co 合金在 960 °C 下的氧化行为；采用 SEM/EDS、XRD 和 Raman 分析氧化膜的组成和结构。对氧化膜的形貌、组成、晶粒尺寸和氧化机制进行分析。结果表明：Ni 金属、Ni-7%Co 和 Ni-15%Co 合金中 Ni 的氧化速率遵循抛物线定律，而 Ni-30%Co 合金中 Ni 的氧化速率遵循三次方定律；合金中 Co 含量越高，Ni 的氧化速率就越快。金属含量分析表明：位于氧化膜下方的合金中 Co 元素有缺失，而且在位于氧化膜外侧的地方 Co 元素逐渐聚集。

关键词：Ni-Co 合金；电沉积；高温氧化

(Edited by YANG Hua)